

MAGYAR ÁLLAMI
EÖTVÖS LORÁND
GEOFIZIKAI INTÉZET

**GEOFIZIKAI
KÖZLEMÉNYEK**

ВЕНГЕРСКИЙ
ГЕОФИЗИЧЕСКИЙ
ИНСТИТУТ
ИМ Л. ЭТВЕША

**ГЕОФИЗИЧЕСКИЙ
БЮЛЛЕТЕНЬ**

G E O P H Y S I C A L

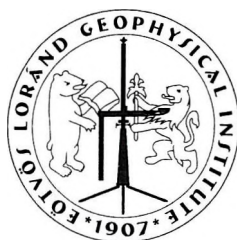
T R A N S A C T I O N S

EÖTVÖS LORÁND GEOPHYSICAL INSTITUTE OF HUNGARY

CONTENTS

Assessment of the location efficiency of the Hungarian seismic monitoring network using various hypocentre determination programs	<i>Z. Bus,</i> <i>P. Mónus,</i> <i>L. Tóth</i>	3
Modelling of cone penetration electric tool field	<i>L. Balázs</i>	19

VOL. 45. NO.1. OCTOBER 2005. (ISSN 0016-7177)



TARTALOMJEGYZÉK

A magyar szeizmológiai állomáshálózat lokalizációs pontosságának vizsgálata különböző hipocentrum-meghatározó programokkal	<i>Bus Z., Mónus P., Tóth L.</i>	16
Penetrációs elektromos szonda modellezése	<i>Balázs L.</i>	35

Assessment of the location efficiency of the Hungarian seismic monitoring network using various hypocentre determination programs

Zoltán BUS*, Péter MÓNUS*, László TÓTH*

A number of strong experimental explosions were detonated in Hungary during the years 1999 and 2000. The seismic magnitude of many of the explosions was large enough to trigger the stations of the Hungarian seismic monitoring network. Arrival time data of seventeen events have proved to be sufficient for calculation purposes. These data together with the ground truth information provided by the organisers of the 'CELEBRATION 2000' Seismic Experiment gave an exceptional chance to test the detection threshold of the seismic monitoring network and to assess its location efficiency. The hypocentral parameters were determined by means of four location programs: HYPO71, HYPOELLIPSE, HYPOINVERSE and JHVINV (the first three are one-dimensional, the fourth is three-dimensional software based on the joint hypocentral-velocity inversion algorithm).

The results show that while the quality of the solutions gained by 1-D methods is more or less similar in each case, the tomographic inversion (JHVINV) improved the precision of hypocentre location in the majority of cases. The root mean square (RMS) of the horizontal errors for JHVINV is 3.1 km (more than 50% better than that of the best one-dimensional procedure), the RMS error of hypocentre depth determination is around 7.6 km (which represents an improvement of 35%).

The seismic magnitudes of the recorded explosions were rather small, ranging from 0.7 to 2.6 on the ML scale, confirming the fairly good detection capability of the network in large areas of Hungary that had earlier been estimated purely from background noise data.

Keywords: earthquakes, CELEBRATION 2000, tomography, inversion

1. Introduction

Earthquake location is one of the most fundamental problems of observational seismology. In this context, location means the determination of hypocentral parameters; in other words, the spatial coordinates of the hypocentre and the earthquake origin time. Usually, during the location procedure the earthquake sources are considered pointwise and the compu-

* HAS GGRI Seismological Observatory, H-1112, Budapest, Mérédek u. 18.

Manuscript received (revised version): 19 July, 2002.

tation is performed using the arrival time data of P - and S -waves, the known station coordinates, and a reliable velocity model.

The precision of earthquake location depends on several factors. It is influenced by the error of the phase readings, the number and distribution of seismological stations providing arrival time data, and the accuracy of the model describing the velocity structure between the source and receivers. As it is difficult to improve the quality of phase readings (which is limited mainly by the signal-to-noise ratio) and the station distribution is given, the easiest way to get better location results is to construct a more realistic velocity model, i.e. one that utilizes models of two or three dimensions. In routine work, one-dimensional velocity models are generally used for hypocentre location, although in the last decades (thanks to tomographic methods) locations based on three-dimensional velocity models are becoming more and more widespread.

The series of experimental explosions detonated in Hungary in 1999 and 2000 gave an exceptional opportunity to test the detection threshold of the seismic monitoring network together with its location efficiency and to compare the performance of location programs. The hypocentral parameters were determined by means of four programs: HYPO71, HYPO-ELLIPSE, HYPOINVERSE and JHVINV.

2. Hungarian seismic monitoring network

In the year 2000, the Hungarian seismic monitoring network comprised 16 seismometer stations belonging to and operated by different organisations [TÓTH et al. 2001].

The core of the system is the Paks micro-seismic monitoring network of eight seismometer stations (PKS2, PKS6, PKS7, PKS8, PKS9, PKSC, PKSM, PKSN), located within a radius of about 100 km from the Nuclear Power Plant at Paks (which is situated approximately in the centre of Hungary) and one additional station in Budapest (BUD) where the data centre is sited and the collected data are analysed [TÓTH, MÓNUS 1997].

Two relocated stations from the Paks network and one additionally installed station form the Üveghuta micro-seismic monitoring network of three seismometer stations (RHK1, RHK2, RHK3), located in the vicinity of the potential nuclear waste disposal site at Üveghuta (situated in the southern part of Hungary).

One broad-band (PSZ), four short period digital (BUD, GYL, PENC, SOP) stations, and one long period analogue (BUD) stand-alone station support the local networks.

The estimated detection capability of the monitoring network with average noise conditions, supposing that at least four stations are needed for origin determination, is typically around 1.5–2.0 ML — somewhat lower in the middle of the country and a little higher towards the border regions (see *Fig. 1*). This means that in most parts of the country it is very unlikely that events that may be felt go undetected by the monitoring network.

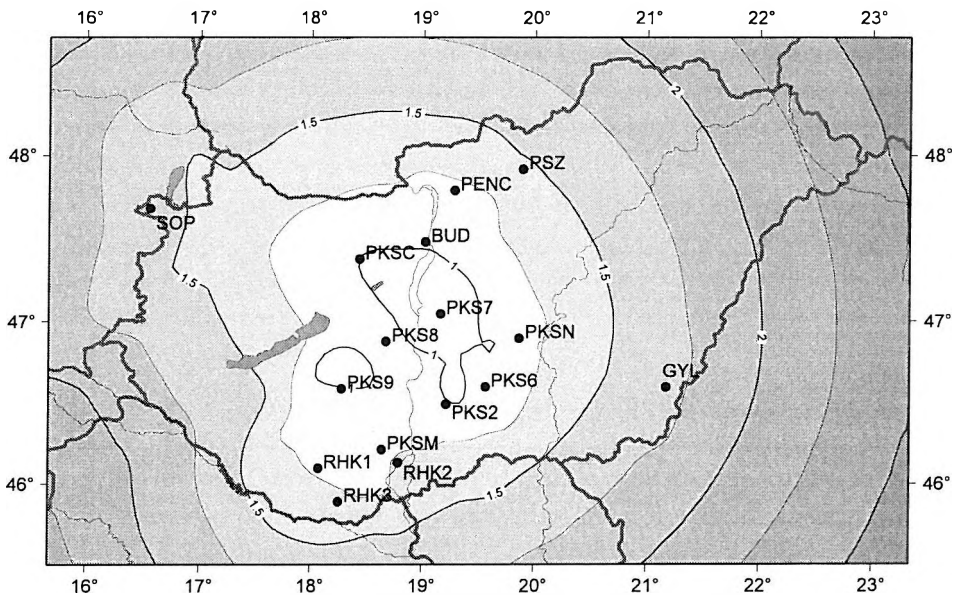


Fig. 1. Seismograph stations and detection capability with average noise conditions of the Hungarian seismic monitoring network. Contour values are Richter local magnitudes (ML). (See TÓTH et al. [2001] for details.)

1. ábra. A magyar szeizmológiai hálózat állomásai, valamint a hálózat érzékelési képessége átlagos zajviszonyok mellett. A kontúrvonalak a Richter-féle magnitúdó (ML) értékeit mutatják (részletesen lásd: TÓTH et al. [2001])

3. Seismic sources

In the autumn of 1999, the Eötvös Loránd Geophysical Institute (ELGI) fired four experimental explosions in Hungary (in the territory of

Transdanubia). All of these events were identifiable based on the data of seismological stations in Hungary and in the surrounding countries.

In the summer of 2000, in the framework of an international project called ‘CELEBRATION 2000’ Seismic Experiment [GUTERCH et al. 2000] many large shots were fired across Europe. Altogether 34 explosions were detonated in Hungary of which 15 could be identified. The weight of charges was between 300 kg and 750 kg. *Table I* shows the data (date, time, code name and location) of the shots, which are in order of the firing times.

4. Software for location

The computer programs for hypocentre location are usually rather complicated (both in capability and in parametrisation), so only the most important features will be outlined here.

4.1 HYPO71

HYPO71 can be considered as the ‘classic’ computer program for determining hypocentre, magnitude and first motion pattern of local earthquakes. Its first version was published in 1971 by LEE and LAHR. Since 1971 several improved versions have been released. Nowadays, HYPO71 is still one of the most popular location programs in observatory practice; it is used for routine earthquake location in Hungary, as well. A detailed description of the software can be found in LEE and LAHR [1975].

By means of HYPO71, weights can be assigned to the arrival data (e.g. according to their reading clarity), and the station delays can be taken into account as well. Theoretical travel times are determined from a horizontally-layered velocity structure with constant velocity in the layers. HYPO71 uses Geiger’s method to find the hypocentre parameters (minimizing the sum of weighted-squared residuals between the observed and the theoretical travel times). HYPO71 is the common precursor of a number of other location software programs.

4.2 HYPOELLIPSE

The HYPOELLIPSE program can be used for determining the hypocentres and magnitudes of local or near regional earthquakes. It also applies Geiger’s method and additionally computes the 68% confidence

Date	Time	Code	Latitude(°)	Longitude(°)
07-09-1999	20: 30: 00	ELGI-1	46.7944	17.9864
09-09-1999	20: 30: 00	ELGI-2	46.5236	16.8614
09-09-1999	20: 45: 00	ELGI-3	47.5528	16.9067
09-09-1999	21: 00: 00	ELGI-4	46.1147	18.7078
07-06-2000	21: 15: 00	1-505	47.4165	19.7832
23-06-2000	21: 15: 00	1-703	46.7858	16.5054
23-06-2000	21: 30: 00	1-804	47.4027	17.2836
23-06-2000	21: 45: 00	1-806	46.9971	17.7194
23-06-2000	22: 30: 00	1-103	47.6294	18.1542
24-06-2000	00: 45: 00	1-803	47.5503	16.9048
24-06-2000	01: 30: 00	1-705	46.3305	17.0320
24-06-2000	21: 15: 00	1-706	46.1307	17.2729
24-06-2000	21: 30: 00	1-504	47.1557	19.5413
24-06-2000	21: 45: 00	1-809	46.3494	18.4797
25-06-2000	00: 00: 00	1-707	45.9885	17.4476
25-06-2000	21: 15: 00	1-501	46.1136	18.7081
25-06-2000	21: 30: 00	1-808	46.6388	18.1728
25-06-2000	21: 45: 00	1-807	46.7936	17.9852
25-06-2000	22: 15: 00	1-502	46.3879	18.9136

Table I. Parameters of the ELGI and 'CELEBRATION 2000' shots (date, time (GMT), code name, latitude and longitude)

I. táblázat. Az ELGI és a "CELEBRATION 2000" robbantásainak paramétereit (dátum, időpont (GMT), a robbantás kódja, szélesség és hosszúság)

ellipsoid. Travel times are determined from a horizontally-layered velocity structure as in HYPO71, but in this case the linear increase of velocity with depth is also permitted. Alternatively a previously generated travel time table can be applied. Arrival times of refracted phases (e.g. P_n) — even at

distances where they do not arrive first — can also be used. The data can be weighted according to their reading clarity (quality weighting), epicentral distance and residual. The HYPOELLIPSE program was developed by LAHR [1999].

4.3 HYPOINVERSE

HYPOINVERSE uses the singular value decomposition (SVD) technique to solve the linearized system of equations of Geiger. Homogeneous layers and models with linear velocity gradient within layers can be applied and the model can include a low velocity zone. Different models for regions with different geological and geophysical properties can be used. The data can be weighted in five different ways, viz. by station, *S*-phase, reading, distance, and residual weights. The program can compute the magnitude of the event, as well. HYPOINVERSE was written by KLEIN [1978].

4.4 JHVINV

The tomographic inversion program JHVINV (written by one of the present authors (Z. B.)) enables the hypocentres to be determined together with three-dimensional *P*-wave velocity distribution. The software is based on the joint velocity–hypocentre inversion technique of THURBER [1993]. The starting one-dimensional model was determined by a genetic algorithm, the initial constraints were based on a priori information. The velocity structure is modelled on a non-uniform, Cartesian grid of nodes. *P*-wave velocity values are assigned to every node, the velocity between the grid points has been computed by tri-linear interpolation.

It is necessary to repeat the linear inversion procedure to get an appropriate solution. During the iteration, the solution of the previous iteration step becomes the initial model for the next one. The *F*-test known from statistics helps to decide when to stop the iteration. A detailed description of the method, the data and the inversion parameters can be found in BUS [2001]. The so called ‘coarse’ velocity model defined in that publication was utilized during our computations.

5. Computations

In each one-dimensional computation the same velocity model was applied; in other words, we used the three-layered crustal and upper mantle model of the Pannonian basin constructed by MÓNUS [1995] which was determined using the travel times of several hundred local and regional events. The initial velocity model of JHVINV was constructed by the previously mentioned genetic algorithm. The initial hypocentral depth was set to 10 km for each 1-D software.

Determination of the initial hypocentral parameters for JHVINV was more complicated. We decided to use the output of the 1-D method giving the best solution for the starting position of epicentres, even so the initial hypocentral depth was set again to 10 km. The quality of the 1-D solutions was assessed on the basis of the number of cases when a particular method gave the best epicentral location and the root mean square (RMS) values of horizontal and vertical errors.

As the programs have a lot of controlling parameters, all of them were set as close as possible in each case. Although most of these programs have the capability to compute the magnitude of earthquakes, this feature was not evaluated in this paper.

Each 1-D program uses both the *P*- and *S*-wave arrival data, while JHVINV uses only *P*-waves' first arrival times.

6. Results

Figs. 2, 3 and 4 display the epicentres computed by various methods together with the true locations. The horizontal and vertical errors of the locations for each hypocentre determination method are shown in *Table II*. The bold numbers in the table mark which 1-D method gave the best result for a given shot. Out of the 19 studied events, two have a horizontal error larger than 10 km (ELGI-2 and 1-806), so these shots will be omitted from the further analysis. The main factor in testing the quality of the results was the horizontal error (the horizontal distance between the true and computed epicentre), as theoretically the hypocentre depth determination has the greatest uncertainty. The root mean square values (RMS) of the horizontal and vertical errors have been calculated for all the analysed 17 events (*Table III*). The horizontal and vertical RMS values will be marked hereafter as RMS-H and RMS-Z, respectively.

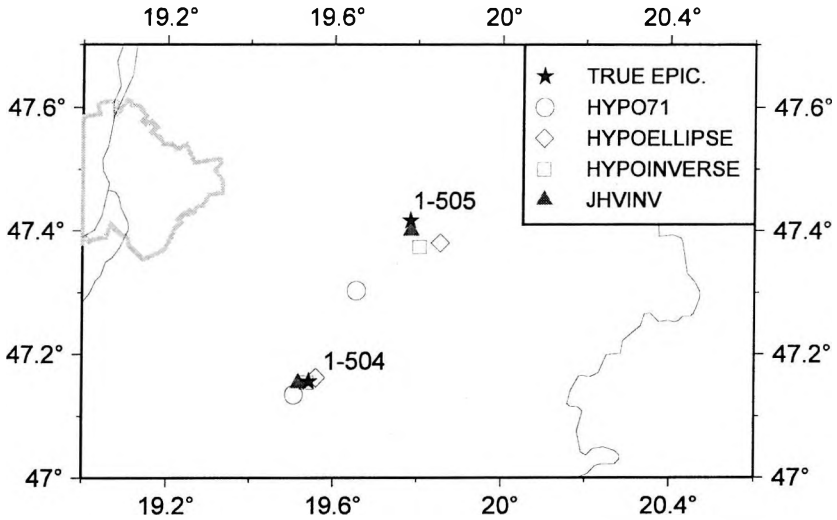


Fig. 2. Distribution of true epicentres and epicentres gained by HYPO71, HYPOELLIPSE, HYPOINVERSE and JHVINV in the vicinity of Budapest

2. ábra. Valós és számított (HYPO71, HYPOELLIPSE, HYPOINVERSE, JHVINV) epicentrum-eloszlás a Budapest környéki robbantások esetében

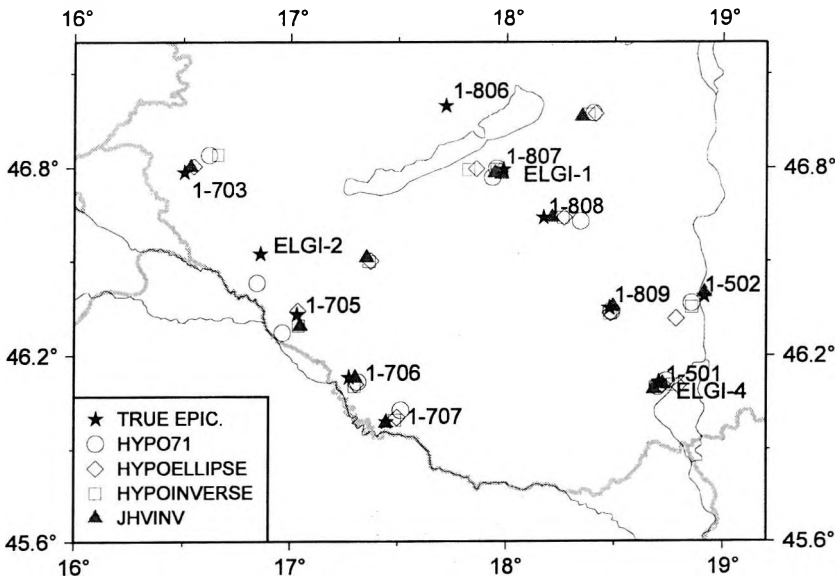


Fig. 3. Distribution of true epicentres and epicentres gained by HYPO71, HYPOELLIPSE, HYPOINVERSE and JHVINV in the southwestern part of Hungary

3. ábra. Valós és számított (HYPO71, HYPOELLIPSE, HYPOINVERSE, JHVINV) epicentrum-eloszlás a délnyugat-magyarországi robbantások esetében

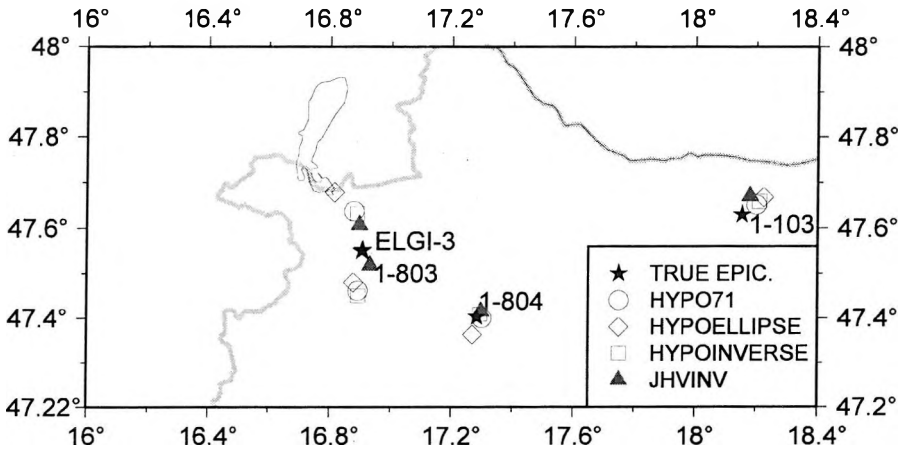


Fig. 4. Distribution of true epicentres and epicentres gained by HYPO71, HYPOELLIPSE, HYPOINVERSE and JHVINV in the northwestern part of Hungary

4. ábra. Valós és számított (HYPO71, HYPOELLIPSE, HYPOINVERSE, JHVINV) epicentrum-eloszlás az északnyugat-magyarországi robbantások esetében

With regard to the results, HYPO71 gave the best epicentre determination in five cases, HYPOELLIPSE and HYPOINVERSE proved themselves to be the best equally in six cases. The RMS–H was the smallest in the case of HYPOINVERSE software. The vertical errors were the smallest for HYPOINVERSE, while the largest for HYPOELLIPSE. The several 10.0 km depth values in the case of HYPO71 can be explained by the fact that it is apt to hold the original initial depth if no significant improvement occurs during the iteration. The RMS–Z values of HYPO71 and HYPOINVERSE are almost equal. The large RMS–Z value of HYPOELLIPSE is caused by the 84 km depth value of shot 1–705, the other two one-dimensional methods gave a value of 10.0 km. Comparing the data in Table III, we can conclude that performances of the one-dimensional methods are more or less similar. However HYPOINVERSE performed slightly better, its output was chosen to be the input of JHVINV. In the case of JHVINV the RMS–H value improved by 53%, while RMS–Z improvement was around 35%. We found depth values of good quality for two shots, viz. 1–703 and 1–803; notably the horizontal errors are not particularly good in these cases.

Table II.

	HYPO71		HYPOELLIPSE		HYPOINVERSE		JHVINV	
	Δh (km)	Δz (km)						
ELGI-1	2,5	10,0	1,4	15,0	2,4	11,6	3,3	9,0
ELGI-2	10,4	10,0	39,2	75,1	38,6	75,3	37,6	14,2
ELGI-3	9,6	10,0	15,6	17,8	9,0	9,8	6,2	4,6
ELGI-4	1,8	10,0	1,5	10,4	2,3	11,1	3,2	7,3
1-505	15,9	14,1	6,6	21,7	5,0	20,6	1,8	11,4
1-703	10,6	1,1	4,0	0,0	13,4	0,2	2,9	0,0
1-804	1,2	10,0	4,5	7,7	1,0	10,4	1,7	4,4
1-806	52,0	0,8	52,7	0,0	50,3	0,0	48,0	0,0
1-103	4,2	13,0	6,8	12,1	5,3	9,0	4,9	6,0
1-803	9,9	0,8	7,9	0,0	11,1	0,0	4,1	1,3
1-705	8,4	10,0	1,3	83,7	3,9	10,0	4,1	4,4
1-706	3,7	25,2	3,5	18,1	3,8	16,7	2,4	13,7
1-504	3,6	17,8	1,5	18,8	0,4	16,8	1,9	9,9
1-809	1,2	10,0	1,7	10,1	1,7	8,9	1,2	7,6
1-707	6,7	7,9	4,1	10,5	3,0	9,8	0,5	6,6
1-501	2,7	8,9	7,0	6,6	4,8	7,8	1,4	6,6
1-808	13,0	10,0	7,4	13,1	6,9	12,1	3,0	4,4
1-807	4,7	10,0	9,5	12,0	12,2	11,1	1,8	6,5
1-502	5,0	13,6	12,5	19,4	5,7	14,5	1,2	11,3

Table II. Horizontal and vertical errors for the one-dimensional (HYPO71, HYPOELLIPSE, HYPOINVERSE) and the tomographic (JHVINV) methods

II. táblázat. Az egyes hipocentrum-meghatározások horizontális és vertikális hibája az egydimenziós (HYPO71, HYPOELLIPSE, HYPOINVERSE) és a háromdimenziós (JHVINV) módszerek esetében

	RMS	
	Δh (km)	Δz (km)
HYPO71	7.5	12.0
HYPOELLIPSE	7.0	24.2
HYPOINVERSE	6.6	11.7
JHVINV	3.1	7.6

Table III. Root mean square values of horizontal and vertical errors for the given location programs

III. táblázat. A helymeghatározás horizontális és vertikális hibáinak négyzetes középértéke a különböző hipocentrum-számító programok esetében

The results of tomographic inversion show that the accuracy of the location improved in 10 cases from the 17 (59%, marked by underlined numbers in the JHVINV's Δh column in Table II), if we compare to the best 1-D values and became better in 12 cases (71%, the ones marked by underlined numbers together with explosions 1–103 and 1–809) if we compare to the results of HYPOINVERSE. The horizontal error of the most accurate JHVINV location was 0.5 km. The histogram of horizontal errors of the results of the JHVINV program can be seen in Fig. 5. It shows that the most populated interval can be found between 0 and 2 km. The spatial distribution of horizontal errors is shown in Fig. 6, from which we

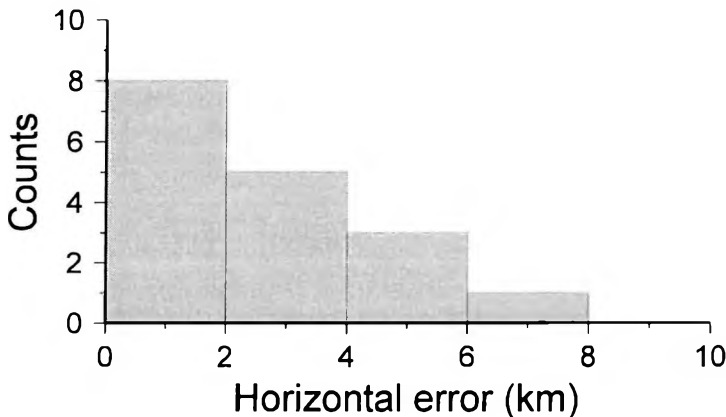


Fig. 5. Histogram of horizontal errors for the tomographic hypocentre location
5. ábra. A tomografikus hipocentrum-meghatározás horizontális hibáinak hisztogramja

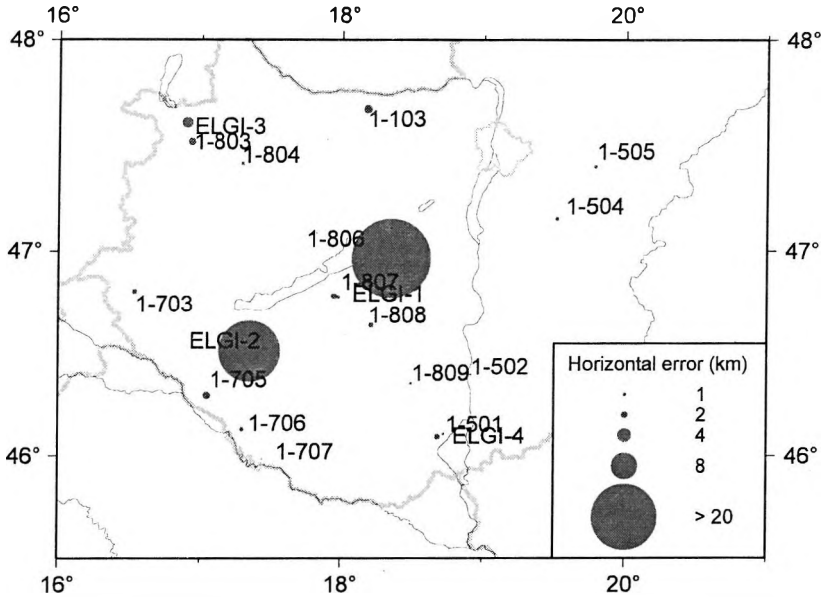


Fig. 6. Horizontal error distribution for the tomographic hypocentre location
 6. ábra. A tomografikus hipocentrum-meghatározás horizontális hibájának területi eloszlása

can conclude that the size of horizontal errors does not depend strictly on the event's relative position to the seismological stations.

The weak location quality of the two shots ELGI-2 and 1-806 can be explained in a different way. In the case of ELGI-2 the probable cause of the poor location is the small number of available data. In the second case the quantity of data was sufficient, but the earthquake location programs have probably been trapped by one of the local minima of the problem. This hypothesis can be proved by substituting the real location into the programs whereupon we get similar residuals as in the mislocated case.

7. Conclusion

Although the seismic magnitudes of the recorded explosions were rather small, the average horizontal location error of the network proved to be around 3 km. The explosion tests also confirm the detection efficiency of the monitoring network (typically around 1.5–2.0 ML) calculated earlier from background noise data.

Comparison of three one-dimensional and one three-dimensional hypocentre location programs indicates that the three-dimensional tomographic location procedure based on the simultaneous hypocentre–velocity inversion improved the accuracy of epicentre location by more than 50% and the hypocentral depth determination by 35% in comparison to the best of the one-dimensional methods. The performance of the 1-D programs tested was more or less identical. We found no significant correlation between the location accuracy and the position of epicentres. Our results showed that the error of hypocentral depth determination can be significant even when the horizontal location is very accurate.

Acknowledgements

The authors are grateful to Endre Hegedűs (ELGI) for providing the parameters of the ELGI and ‘CELEBRATION 2000’ shots. The Paks Microseismic Monitoring Network Project is sponsored by Paks Nuclear Power Plant Ltd. and was carried out by the GeoRisk Earthquake Research Institute.

REFERENCES

- BUS Z. 2001: Tomographic imaging of three-dimensional *P*-wave velocity structure beneath the Pannonian basin. *Acta Geod. Geoph. Mont.*, **36**, pp. 189–206
- GUTERCH A., GRAD M., KELLER G. R., POSGAY K., VOZÁR J., SPICAK A., BRUECKL E., HAJNAL Z., THYBO H., OGUZ S. 2000: CELEBRATION 2000: Huge seismic experiment in Central Europe. *Geologica Carpathica*, **51**, pp. 413–414
- KLEIN F. W. 1978: Hypocenter Location Program HYPOINVERSE, Part I: Users Guide to Versions 1, 2, 3 and 4. U. S. Geol. Survey Open File Rep., pp. 78–694
- LAHR J. C. 1999: HYPOELLIPSE: A Computer Program for Determining Local Earthquake Hypocentral Parameters. Magnitude and First-Motion Pattern. U. S. Geol. Survey Open File Rep., pp. 23–99
- LEE W. H. K., LAHR J. C. 1975: HYPO71: A computer program for determining hypocenter, magnitude and first motion pattern of local earthquakes. U. S. Geol. Survey Open File Rep., pp. 75–311
- MÓNUS P. 1995: Travel time curves and crustal velocity model for the Pannonian basin. HAS GGRI Technical Report
- THURBER C. H. 1993: Local earthquake tomography: velocities and V_p/V_s - theory. *In*: IYER H. M., HIRAHARA K. (eds): *Seismic tomography: theory and practice*. Chapman and Hall, London, pp. 563–583

- TÓTH L., MÓNUS P. 1997: The micro-seismic monitoring network of the Paks NPP. *In: Seismic Safety of the Paks Nuclear Power Plant*. Akadémiai Kiadó, Budapest, pp. 113–121
- TÓTH L., MÓNUS P., ZSÍROS T., KISZELY M., KOSZTYU Z. 2001: Hungarian Earthquake Bulletin, 2000. GeoRisk, Budapest, 98 p.

A magyar szeizmológiai állomáshálózat lokalizációs pontosságának vizsgálata különböző hipocentrum-meghatározó programokkal

BUS Zoltán, MÓNUS Péter és TÓTH László

Szeizmikus refrakciós mérések keretében 1999 és 2000 folyamán számos nagyerejű kísérleti robbantást hajtottak végre Magyarország területén. A magyar szeizmológiai hálózat által gyűjtött adatok 19 robbantás esetében tették lehetővé a hipocentrumok meghatározását. Az eredmények a "CELEBRATION 2000" szervezői által biztosított robbantási paraméterekkel együtt kivételes lehetőséget teremtettek a magyarországi állomáshálózat helymeghatározási pontosságának és érzékelési képességének vizsgálatához. A mesterséges rengések fészekparamétereit négy különböző számítógépes programmal határoztuk meg, melyek közül három egydimenziós (HYPO71, HYPO-ELLIPSE, HYPOINVERSE), egy pedig háromdimenziós (JHVINV) sebességmodellen alapuló lokalizációt tett lehetővé.

Az eredmények azt mutatják, hogy míg az 1-D számítások pontossága többé-kevésbé megegyezik, addig a 3-D tomográfiai eljárás jelentősen jobb eredményeket szolgáltatott a számítások többségében. A horizontális helymeghatározás hibájának négyzetes középértéke (RMS) a háromdimenziós esetben 3,1 km (amely több mint 50 százalékkal jobb, mint a legpontosabb egydimenziós eljárásé), a hipocentrum mélységének RMS hibája 7,6 km (amely 35 százalékos javulást jelent az egydimenziós esethez képest).

A regisztrált robbantások magnitúdója meglehetősen kicsi volt (0,7–2,6 a Richter-skálán), érzékelésük ténye igazolta a pusztán a háttérzaj adatokból nyert érzékelésiképesség-bebecslés megbízhatóságát.

ABOUT THE AUTHORS



Zoltán Bus received his M.Sc. (1994) and Ph.D. (2005) in geophysics from the Eötvös Loránd University. Since 1994 he has been working at the Seismological Observatory of the Geodetic and Geophysical Research Institute of the Hungarian Academy of Sciences. His main fields of interest are travelttime tomography, receiver function analysis and deterministic seismic hazard assessment. He is a member of the Association of Hungarian Geophysicists.



Péter Mónus received his M.Sc. (1980) in geophysics from the Eötvös Loránd University, Budapest. In 1980 he joined the Seismological Observatory of the Hungarian Academy of Sciences at Budapest. Since this date he is working there as a seismologist. His main interest is in microseismic observations, earthquake focal parameter determination. He is a member of the EAAE.



László Tóth graduated (M.Sc) in geophysics and meteorology at Eötvös University, Budapest in 1979. Having completed post graduated scholarships at NORSAR, Norway and Grafenberg, Germany, got Ph.D. in seismology, Eötvös Univ., Budapest (1984).

Served as government expert at the Comprehensive Test Ban Treaty negotiations in Geneva (1987–1996) until its completion and participated several workshops and seminars related to seismological verification of a CTBT. Has been working as consultant for the Comprehensive Test Ban Treaty Organization since 1998. Participated several local projects on seismic hazard assessment, observation of underground nuclear tests, GSETT, PHARE projects and EU Projects. Main fields of interest are earthquake seismology, detection seismology, seismicity, seismic hazard assessment, earthquake monitoring and seismic data processing.



Modelling of cone penetration electric tool field

László BALÁZS*

Cone penetration sounding is one of the most important information sources in shallow geophysical research. It is pointed out, however, that efficient interpretation requires highly reliable modelling of the sonde operation. The special difficulties that arise when modelling the field of the cone penetration electric logging tool originate from the disturbing effect of cone and shaft. Large conductive inhomogeneities arise that tend to adversely affect the current density distribution and potential field generated by the active electrodes as well as the measured apparent resistivity value. It is emphasized that great care must be taken in providing the most appropriate extended electrode model that is required, in order to calculate the surface current density distribution, which is the key function for estimating the long electrode potential field. From the mathematical point of view, the problem can be formulated as a Fredholm-type integral equation of the first kind with a weakly singular kernel function.

In this article, we have built up step by step the mathematical model of the penetration sonde starting with the simplest ring electrode model; we then derived the current density cylindrical electrode; using the results, we next calculated the single uniform surface potential electrode field; finally, we modelled the field of the whole electrode system. The single electrode field was a reference case for which we approximated the electrode surface current density distribution by two methods, viz. step function and Fourier series. As a result, the real electric tool current density and potential distribution were estimated in a homogeneous medium; this procedure is useful for interpreting cone penetration logs, taking into account the effect of varying length shaft, and also for tool planning. If the core function is modified, the modelling can easily be extended to a radially inhomogeneous medium, approximating the compaction around the tool.

Keywords: cone penetration, sounding, electrical logging

* Budapest University of Technology and Economics – Institute of Nuclear Technics, H-1111 Budapest, Műgyetem rkp. 3-9. e-mail: balazs@reak.bme.hu

Manuscript received (revised version): 4 March, 2005.

1. Introduction

If the size of the given medium inhomogeneities (including the sonde body) is comparable with the size (length) of the electrodes, then great care must be taken to ensure that the most appropriate extended electrode model is selected for calculating the logging tool field; inevitably, if the appropriate choice is made this will be more realistic than the often applied point electrode model. In the case of the penetration tool, the cone and shaft form large conductive inhomogeneities that behave like long passive electrodes, thereby exerting a significant effect on the potential field. It means that the sum of the current on the shaft and cone (as a coupled passive electrode) is equal to zero. By no means should the cone and shaft effect be neglected when calculating the sonde constant, the apparent resistivity, the transfer resistances, and in interpreting the log.

2. The basic problem

In the modelling of direct current electrode systems, the Laplace equation must be solved in the medium in which the electrodes are embedded, excluding the current source region. In the case of cylindrical symmetry outside the electrodes the potential function ($V(r, z)$) fulfils:

$$\frac{1}{r} \frac{\partial V}{\partial r} + \frac{\partial^2 V}{\partial r^2} + \frac{\partial^2 V}{\partial z^2} = 0 \quad , \quad (1)$$

where r and z are cylindrical co-ordinates.

At the surface of the electrodes and at the boundary of the medium's inhomogeneities, the appropriate boundary conditions determine the free parameters of the general solution. At the electrode surface, the boundary conditions may refer to the surface potential (Dirichlet problem) or to the current density (Neumann problem), sometimes complemented by the electrode current as a normalization factor (Tikhonov-type normalization).

If one neglects the angle variable, the general solution can be formulated for the homogeneous region of the given medium by the appropriate Bessel functions (J_0, N_0, K_0, I_0):

$$V(r, z) = \int_0^{\infty} [A(m) \operatorname{ch}(mz) + B(m) \operatorname{sh}(mz)] [C(m) J_0(mr) + D(m) N_0(mr)] dm \quad (2a)$$

or in an equivalent form:

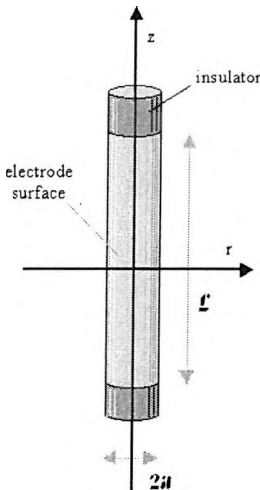
$$V(r, z) = \int_0^{\infty} [A(m) \cos(mz) + B(m) \sin(mz)] [C(m) I_0(mr) + D(m) K_0(mr)] dm \quad (2b)$$

where $A(m)$, $B(m)$, $C(m)$, $D(m)$ are weight functions, and m is the space frequency. The form of the general solution is a superposition of the eigenfunctions of differential equations derived from the Laplacian one by the separation of variables. The first form (Eq. 2a) is suitable for vertical inhomogeneities, the second (Eq. 2b) for radial ones. The general solution could be simplified when the potential vanishes in infinity, or remains finite in the centre of the co-ordinate system, or further symmetry can be assumed.

For a central single electrode in a homogeneous medium, the solution can be simplified to the form

$$V(r, z) = \int_0^{\infty} A(m) K_0(mr) \cos(mz) dm \quad (3)$$

because of the parity requirement of the variable r . The weight function $A(m)$ can be determined from the boundary condition at the source region. If one uses (Eq. 3), it is possible to generate a solution which gives a finite potential on the electrode surface.



3. Electrode model

The starting point of mathematical modelling was the electrode model suggested by DE WITTE [1959]. In this model the infinitely thin conductive cover is mounted on the insulating cylinder (Fig. 1). The extended electrode model outlined in Fig. 1 can be derived from infinitely thin ring electrodes by superposition. The whole electrode system is built up from cylindrical electrodes of different lengths. The tool body as an ideal insulator can

Fig. 1. The electrode model: infinitely thin conductor cover on the insulator body
 1. ábra. Az elektróda modell: elhanyagolható vastagságú vezető burkolat szigetelő hengeren

be characterized by zero radial current density. All the electrodes have uniform surface potential. The active electrodes emit a predefined current, and the surface integral of the passive electrode radial current density is equal to zero.

The first step in constructing the mathematical model is to determine the Green-function belonging to the infinitely thin ring electrode. (With regard to the vertical co-ordinate (z), this is the Dirac-delta source, which generates the Green potential distribution). The Green-function must have a symmetry:

$$G(r, z, z') = G(r, |z - z'|) \quad . \quad (4)$$

Using the Green-function, the electric field of the arbitrary electrode system can be calculated by convolution:

$$V(r, z) = \int_{z' \in \eta} J(z') G(r, z, z') dz' \quad , \quad (5)$$

where η is the finite region on the vertical axis, representing the electrode surfaces; $J(z)$ the vertical current density, which is continuous on η .

The inhomogeneities of the medium can be built into the Green-function.

3.1. The Green-function

At the electrode surface, the current density vector has only a radial component because it is an ideal conductor. The surface integral of the current density is also known as a current of the electrode. Then the equation (boundary condition) for the current density is

$$\delta(z) = -\frac{2\pi a}{R} \left(\frac{\partial V(r, z)}{\partial r} \right)_{r=a} \quad , \quad (6)$$

where R is the resistivity of the medium, a the radius of the electrode. Substituting the symmetric general solution (Eq. 3) to (Eq. 6) gives:

$$\frac{R}{2\pi a} \delta(z) = -\int_0^{\infty} (A(m) I_1(ma) - B(m) K_1(ma)) \cos(mz) m dm \quad . \quad (7)$$

In the case of a homogeneous medium:

$$\frac{R}{2\pi a} \delta(z) = \int_0^{\infty} B(m) K_1(ma) \cos(mz) m dm \quad . \quad (8)$$

The Dirac-delta function on the left side can be expressed by cosine functions, applying the orthogonality:

$$\lim_{z' \rightarrow 0} \frac{1}{\pi} \int_0^{\infty} \cos(mz) \cos(mz') dm = \frac{2\pi a}{R} \int_0^{\infty} B(m) K_1(ma) \cos(mz) m dm \quad . \quad (9)$$

From the equality of parametric integrals, the unknown weight function $B(m)$ can be determined:

$$B(m) = \frac{R}{2\pi^2 am K_1(ma)} \quad . \quad (10)$$

Hence the Green-function for a homogeneous medium, substituting (Eq. 10) to (Eq. 3) is:

$$G(r, z - z') = \frac{R}{2\pi^2 a} \int_0^{\infty} \frac{1}{m K_1(ma)} K_0(mr) \cos(m(z - z')) dm \quad . \quad (11)$$

It should be noted that the Green-function is singular on the surface of an infinitely thin ring electrode (at the point $r = a$), since finite current enters the measured medium from an 'infinitely small' region. Using the Green-function and knowing the vertical current density distribution, one can calculate the potential anywhere in the medium.

Generally speaking, the current density distribution is not known. It can be determined from a Fredholm-type integral equation based on the above-formulated Green-function. Since the electrode is an ideal conductor, the surface potential is constant. Hence the integral equation for a single electrode is given by

$$V(a, z) \Big|_{z \in \eta} = \int_{z' \in \eta} J(z') G(a, z - z') dz' = \text{const.} \quad (12)$$

The kernel function is symmetric and has weak singularity. The weakness of singularity ensures the finite surface potential in the case of a finite electrode (finite radius and length), after the integration given in (Eq. 12).

If we have a multiple electrode system, the integral equation must be completed by the mutual effect of the other electrodes. This effect can be formulated by similar coupled integral equations. Normalizing the solution requires further conditions. If the i -th electrode current (I_i) is known, the normalization is given by

$$I_i = \int_{z' \in \eta_i} J(z') dz' \quad . \quad (13)$$

If the shaft reaches the zero potential point (far surface point), then the shaft electrode potential can be forced to zero. This is the other possible kind of normalization.

The multi-electrode system seems to be an incomplete Dirichlet problem since the potential is known only at a certain region of the tool body (incomplete boundary condition); moreover the measuring point is also on the boundary.

4. The possible way of electrode field calculation

Two main steps are needed to solve the outlined problem: (i) The surface current density is calculated by inverting the integral equation related to the electrode surface potential, (ii) knowing the current density and Green-function, we can calculate the potential by convolution at any point outside the electrode system.

The simplest solution is to partition vertically the extended electrode into constant vertical current density component electrodes. In this way, the current density is approximated by a step function (sampling by step function). The goodness of approximation is determined by the fineness of the partitioning. The integral equation is then approximated by a linear equation system to calculate the vertical current density vector. For normalization the whole current or surface potential is required. The matrix element of the linear equation is derived from the Green-function (at the reference point of the part electrodes). Herewith, we introduce the matrix \mathbf{D} with the components:

$$D_{i,j} = V_{i,j} - V_{i,j+1} \quad (14)$$

where $V_{i,j}$ is the potential originating from the i -th component electrode on the j -th part electrode:

$$V_{i,j} = J(z_i)G(z_i - z_j)$$

where z_i is the vertical co-ordinate of the i -th component electrode. The coefficients in the last row of the matrix referring to the whole electrode current are given by

$$D_{i,N} = 1$$

expressing the normalization, where N is the number of the component electrode. Then the current density vector, \mathbf{J} is derived:

$$\mathbf{J} = \mathbf{D}^{-1}\mathbf{b}, \quad (15)$$

\mathbf{b} represents the boundary conditions on the electrode surface. The components of array \mathbf{b} are zero except the last, which is just the electrode current. If the surface potential is known, the linear equation can be written directly to the potentials. In this case the matrix elements are Green-function values at the distance of the component electrodes. The linear equation system outlined above can also be derived from the conditional extremum of the electrode surface power.

4.1. Potential of the constant current density component electrode

To generate the linear equation system mentioned above, the potential field of the uniform current density component electrode must be calculated. This will be the basis for the numerical treatment of the current density approximation. If the Green-function is known, the potential function of the uniform current density component electrode (L : length, a : radius) field is:

$$V(r, z) = \frac{IR}{2\pi^2 a_0} \int_0^\infty (A(m)I_0(mr) + B(m)K_0(mr)) \cos(mz) \sin\left(\frac{mL}{2}\right) dm. \quad (16)$$

where R is the resistivity of the medium, and I is the electrode current.

In a homogeneous medium the weight function $A(m)$ is equal to zero for each m , and $B(m)$ is the same as in (Eq. 10). As can be seen from (Eq. 16) above, the surface potential of this kind of electrode is not constant. The surface potential and current can be uniform only in the case of an infinitely long electrode. The component electrode reference point in our approximation was the centre of the electrode.

From *Fig. 2*, the convergence of the potential decrement can be realized for electrodes of different lengths which have the same current.

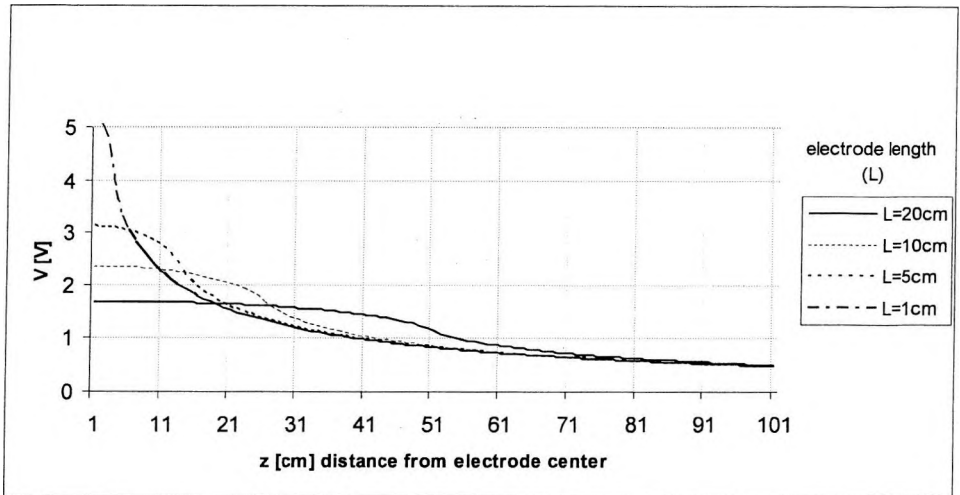


Fig. 2. Potential distribution for uniform current density electrodes of different lengths (radius : 0.025 m, electrode current: 1A)

2. *ábra.* Potenciál eloszlás különböző hosszúságú, egyenletes árameloszlású elektródák esetén ($r=0,025$ m, áramerősség: 1A)

4.2. Approximation of current density for a uniform surface potential electrode

In this section, the whole electrode current density is calculated from component electrode fields.

To check the numerical treatment one should compare the calculated current density with the result originating from different types of approximation. It would be useful if the inverse of the Green-function could somehow be expressed:

$$\delta = G^{-1} * G \quad . \quad (17)$$

In this case the surface current density would be:

$$J = V * G^{-1} = (J * G) * G^{-1} = J * \delta \quad . \quad (18)$$

In a homogeneous medium the inverse can be given in the following form:

$$G^{-1}(a, z) = \text{const} \int_{-\infty}^{\infty} \frac{mK_1(ma)}{K_0(ma)} \cos(mz) \, dm \quad (19)$$

This type of solution requires the whole potential function along the z axis. Because of the 'incomplete boundary condition' and the infinite Green-function, this inverse gives only a poor approximation. Evolving a local inverse with continuous spectra — as formulated in (Eq. 19) — is not possible.

The problem outlined above may be avoided if the unknown current density $J(z)$ is taken in Fourier-series form, i.e. the $J(z)$ and $V(z)$ on the electrode surface are extended periodically outside the electrode region. Thus, the local relationship can be determined between the two local functions. During the current density calculation the convolution is related only to the electrode surface, therefore the infinite periodic extension causes no problem. The basic Fourier period is the electrode length.

If one substitutes the $J(z)$ Fourier-series with unknown coefficients (a_n) into the potential expression (Eq. 12), the following is obtained:

$$V(a, z) = \sum_n a_n \int_0^{\infty} A(m) K_0(ma) \cos(mz) \int_{-L/2}^{L/2} \cos(mz') \cos\left(\frac{2\pi n}{L} z'\right) dz' \, dm \quad (20)$$

It can be seen that the integral transformation defined above (Eq. 20) transfers the constant function ($n = 0$) to the symmetric decreasing function. The zero order approximation is just the uniform current density electrode model. Calculating the second integral, we get:

$$V(a, z) = \sum_n a_n \int_0^{\infty} A(m) K_0(ma) \sin\left(m \frac{L}{2}\right) (-1)^n \frac{2m}{m^2 - \left(\frac{2\pi n}{L}\right)^2} \cos(mz) \, dm \quad (21)$$

where k is the index variable, c_k are the Fourier coefficients of the potential function V ; $B_{k,n}$ are elements of the coupling matrix between current density and potential Fourier harmonics. The potential is expressed as a series of special functions. This basis is not orthogonal. If we transform these functions to the orthogonal Fourier basis we get:

$$V(a, z) = \sum_n a_n \sum_k B_{k,n} \cos\left(\frac{2\pi k}{L} z\right) = \sum_k c_k \cos\left(\frac{2\pi k}{L} z\right) \quad (22)$$

which is just the Fourier-series of surface potential, where:

$$B_{k,n} = \int_0^{\infty} A(m) K_0(ma) \sin^2\left(m \frac{L}{2}\right) (-1)^{n+k} \frac{2m}{m^2 - \left(\frac{2\pi n}{L}\right)^2} \frac{2m}{m^2 - \left(\frac{2\pi k}{L}\right)^2} dm. \quad (23)$$

A symmetrical matrix describes the coupling of the source (current density) and potential spectra. Since the surface potential of the electrode is uniform ($V_f = V(a, z)$; $z \in [-L/2, L/2]$), it means that only the first coefficient differs from zero, hence the Fourier coefficient vector of current density distribution is the following:

$$\mathbf{a} = \mathbf{B}^{-1} \mathbf{c} \quad (24)$$

where the surface potential Fourier coefficients (c_i) expressed by surface potential value (V_f) are:

$$c_i = V_f \delta_{i,0} \quad (25)$$

For comparison, the single electrode current density functions were calculated with different electrode divisions, using (Eq. 15). The estimated current density step functions are displayed in *Fig. 3*.

In *Fig. 4* the current density distribution can be seen derived from Fourier-series approximation for the same electrode as given above. The calculated function is burdened by a slight Gibbs oscillation because of the truncation of the Fourier-series. The values of the two approximations agree at the side of the electrode, but slightly differ in the central part.

5. Modelling of cone penetration sonde

The mathematical model of the electrodes described above is suitable for cone penetration electric tool modelling. The 1 cm uniform partitioning was used in the numerical treatment. In the modelling we ignore the cone bend. (The effect of this geometry can be estimated by two cylindrical electrodes of different lengths). The cone and shaft — because of their connection — have the same surface potential. In the calculation the shaft potential is forced to zero; it means that the shaft is practically infinite (it is connected to the zero potential reference point of the measurement).

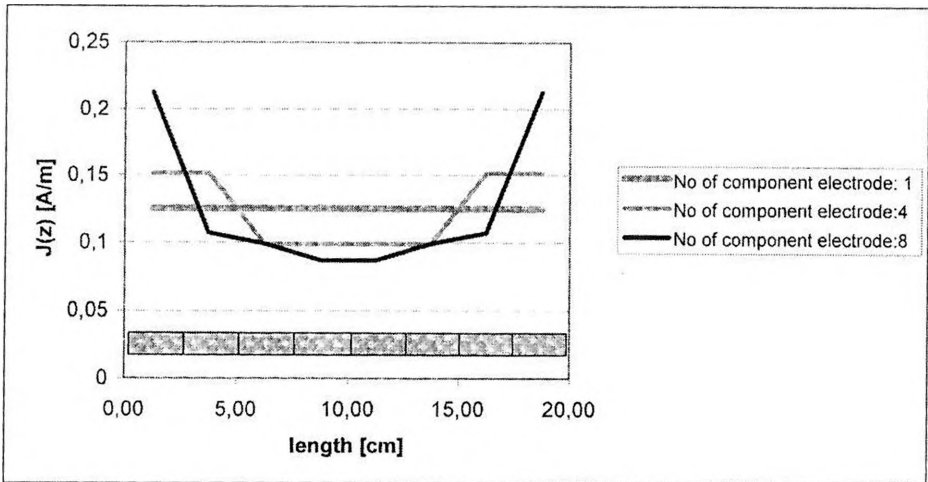


Fig. 3. Electrode surface current density approximation with different electrode divisions. The electrode length was 20 cm, the radius 2.5 cm

3. ábra Felszíni áramsűrűség eloszlás közelítése, az elektróda különböző finomságú felosztásával. Az elektróda hossza 20 cm, sugara 2,5 cm volt

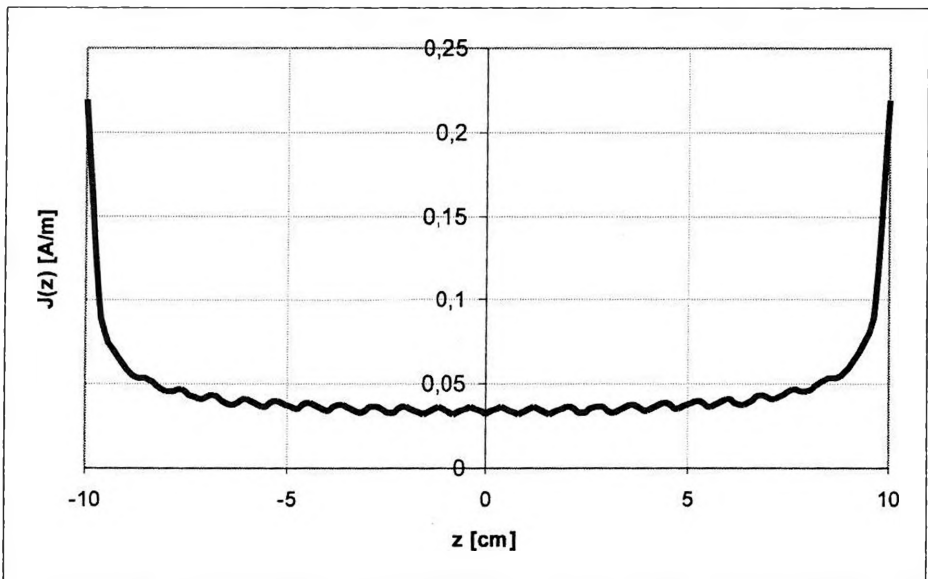


Fig. 4. Electrode surface current density approximation by Fourier series. The electrode length was 20 cm, the radius 2.5 cm

4. ábra. Az elektróda felszíni áramsűrűség eloszlásának közelítése Fourier-sor segítségével. Az elektróda hossza: 20 cm, sugara: 2,5 cm volt

The current of the measuring electrode was zero (passive electrode); the potential of the measuring electrode was calculated by means of the extended electrode model. If the shaft is taken to be of finite length, the current of the shaft-cone system can also be taken as zero, but in this case the surface potential is a little bit above zero. From the boundary conditions, the linear equation system can be derived for the 1 cm long component electrodes. If the equation is solved, the current density vector can be determined.

The result of the step function approximation is displayed in Fig. 5. If the cone and shaft are not connected, negative current density values appear on the end of the cone, and positive values on the end of the shaft. As a consequence of connection and zero potential, the current of the shaft and cone will outflow towards the surface.

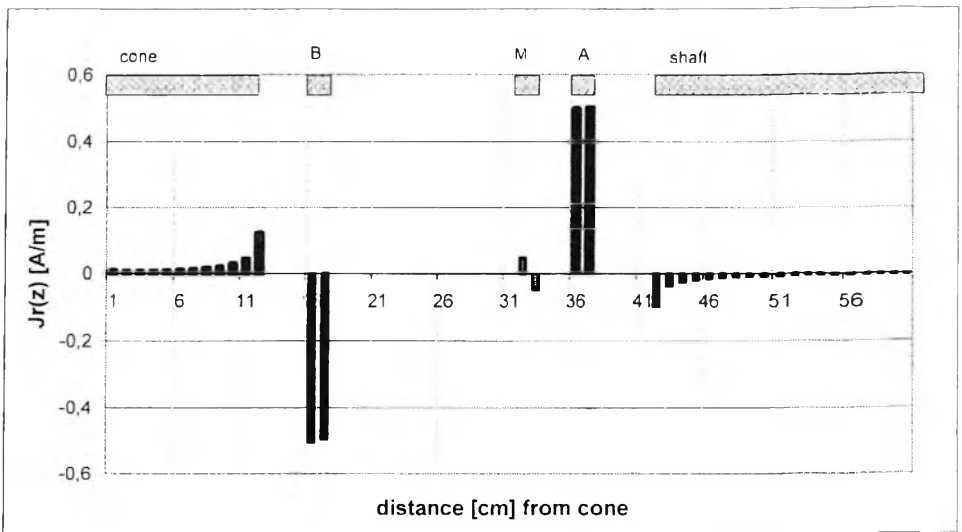


Fig. 5. Surface current density on the penetration tool
5. ábra. Árameloszlás a penetrációs szonda felszínén

From Fig. 5, it can be seen that the shaft-cone system carries the essential part of the current originating from the active electrodes (*A*, *B*). This effect changes the potential at the measuring point (*M*). The current distribution on the active electrode is also asymmetric, as an effect of passive electrodes. The currents of the component electrodes are listed in Table I.

Electrode	Current [A]
M_1	0.0467
M_2	-0.0467
A_1	0.49863
A_2	0.50137
B_1	-0.50459
B_2	-0.49541

Table 1. Currents of component electrodes
1. tábl. Részelektrodák árama

The potential distribution along the sonde axis is shown in Fig. 6. From Fig 6, it can be seen that the potential of the cone–shaft electrode is forced to zero. The potential on the measuring electrode is also constant on the electrode surface. The deviation in measured resistivity caused by the

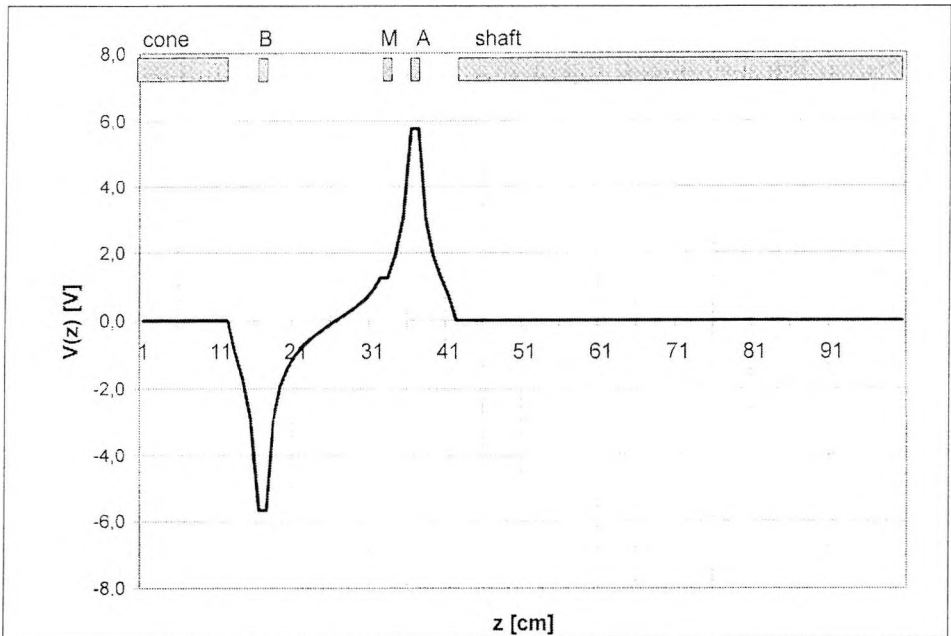


Fig. 6. Surface potential on the penetration tool (infinite shaft approximation)
6. ábra. Potenciáeloszlás a penetrációs szonda felszínén (végtelen fúrósár közelítés)

cone–shaft effect was about 10 %. If the surface potential of the shaft–cone is forced to zero, the solution becomes insensitive to the length of the shaft.

In Fig. 7, the potential distributions from different approximations are compared: point electrode model, extended electrode model without shaft and cone, extended electrode with shaft–cone. Far from the active electrodes all these models give similar results, as can be expected, but close to the active electrodes the difference is significant.

If the effect of the cone–shaft is calculated, the potential at the measuring point (electrode M) in a homogeneous $1 \Omega\text{m}$ resistivity medium is 1.25 V ; neglecting the cone and shaft effect and the local effect of electrode M we get 1.143 V . If the local effect of electrode M is taken into account the measured potential is 1.329 V , since the measuring electrode also modifies the local potential distribution. This effect may be reduced by decreasing the length of the measuring electrode.

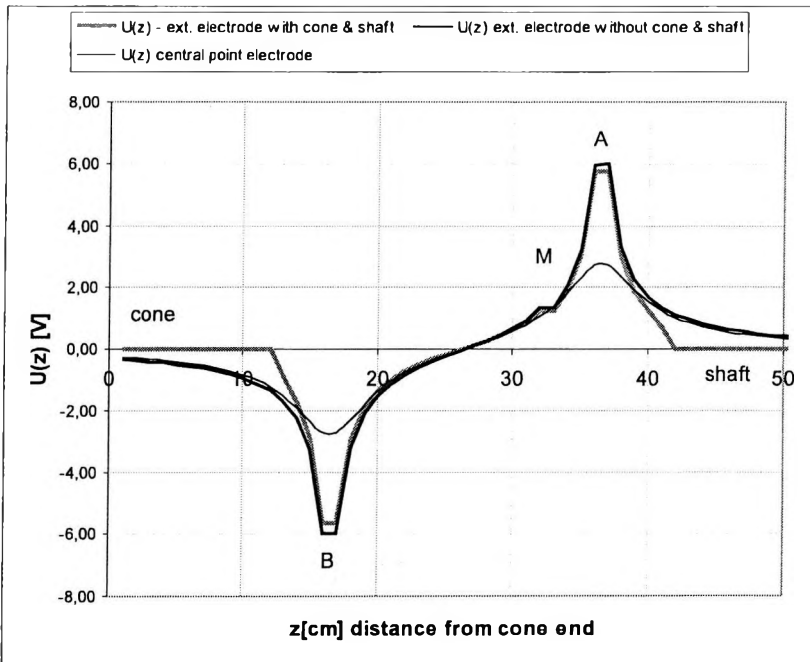


Fig. 7. Surface potential on the penetration tool in different approximations

7. ábra. Potenciál eloszlás a szonda felszínén különböző közelítésekben (pontelektrodákkal, nyújtott elektrodákkal fűrészsár és csúcs nélkül, nyújtott elektrodákkal a csúcs és fűrészsár hatás figyelembe vételével)

Z [cm] from the cone end	$V(z)$	$V(z)$ without cone-shaft	$V(z)$ point electrode
11 (cone)	0.0	-1.129	-1.007
12 (cone)	0.0	-1.365	-1.223
13	-0.9259	-1.706	-1.513
14	-1.702	-2.247	-1.899
15	-2.884	-3.304	-2.362
16 (B)	-5.672	-6.01	-2.736
17 (B)	-5.672	-6.01	-2.717
18	-2.989	-3.22	-2.303
19	-1.928	-2.121	-1.801
20	-1.37	-1.532	-1.373
21	-1.005	-1.139	-1.039
22	-0.7377	-0.8479	-0.7763
23	-0.5264	-0.6147	-0.5631
24	-0.3486	-0.4169	-0.3823
25	-0.1902	-0.2396	-0.222
26	-0.04148	-0.07294	-0.07281
27	0.105	0.09107	0.07281
28	0.2563	0.2597	0.222
29	0.4215	0.4424	0.3823
30	0.6126	0.6516	0.5631
31	0.8624	0.9203	0.7763
32 (M)	1.25	1.329	1.039
33 (M)	1.25	1.329	1.373
34	1.933	2.058	1.801
35	3.042	3.195	2.303
36 (A)	5.759	5.945	2.717
37 (A)	5.759	5.945	2.736
38	3.013	3.291	2.362
39	1.89	2.238	1.899
40	1.248	1.7	1.513
41	0.713	1.36	1.223
42 (Shaft)	0.0	1.125	1.007
43 (Shaft)	0.0	0.9508	0.8437

Table II. Surface potential values in various approximations
 II. táblázat. Szondafelszíni potenciál értékek különböző közelítésben

In *Table II*, the potential values along the sonde surface are tabulated in different approximations. If the cone–shaft is modelled as a passive, zero current electrode, the surface potential will be above zero depending on the shaft length.

6. Conclusions

The electrical model described above is suitable for calculating the tool response in the case of a homogeneous medium and radial inhomogeneity. It is proved by our model of the penetration electrical tool that the cone and shaft effect is important and it must therefore be taken into account in the sonde planning and in the subsequent interpretation of the results.

Acknowledgement

The work outlined in this article was carried out in the framework of the project ‘Theoretical modelling of shallow sounding’ (No: T043748) supported by OTKA.

REFERENCES

- DRAHOS D. 2003: On penetration electric soundings. *Geophysical Transactions* **44**, 3–4, pp. 213–220
- FEJES I., JÓSA E. 1990: The engineering geophysical sounding method: principles, instrumentation, and computerised interpretation, *In* WARD S. H. (ed.): *Geotechnical and environmental geophysics; II, Environmental and groundwater*. Tulsa, Oklahoma pp. 321–331.
- STICKEL J. 1994: *Ergebnisse der strukturgeophysikalischen Messungen am Teststandort Berlin – Schöneiche. Geophysikalische Penetrationsondierungen. Ergebnisbericht Eötvös Loránd Geophysical Institute of Hungary*
- DE WITTE L., GOULD R. W. 1959: Potential distribution due to a cylindrical electrode mounted on an insulating probe. *Geophysics* **XXIV**, 3, pp. 566–579

Penetrációs elektromos szonda modellezése

BALÁZS László

A penetrációs szonda mérések a sekély geofizikai kutatás egyik legfontosabb információ forrásai. A mérési eredmények megfelelő interpretációjához elengedhetetlen a szonda terének megfelelő modellezése. Az elektromos szonda modellezést a csúcs és a fúrósár elektromos teret torzító hatása nehezíti. Ennek leírásához realiztikus nyújtott elektróda modellt kell létrehozni, melynek segítségével számolható a szonda felszíni árameloszlása és a közegbeli potenciál eloszlás.

Matematikai szempontból a feladat egy Fredholm-típusú (elsőfajú), gyengén szinguláris magú integrálegyenlettel fogalmazható meg. A cikkben a matematikai modell kifejlesztésének lépéseit mutatjuk be. Kiindulva egy egyszerű gyűrűelektródból, ebből létrehozva egyenletes felszíni áramsűrűség-eloszlású hengerelektródot, melyből egyenletes felszíni potenciáeloszlású elektródot származtatva eljutunk a teljes elektromos szonda realiztikus modellezéséhez. Az áramsűrűség eloszlást lépcsőfüggvény és Fourier-sor formájában is közelítjük. Az eredmények hasznosak lehetnek a szonda mérési eredményeinek interpretációjában, illetve a szonda fejlesztésben is. A magfüggvény kis módosításával a radiálisan inhomogén közeg (kompakció modellezése) is számítható.

ABOUT THE AUTHORS



László Balázs received his M.Sc. in geophysics from the Eötvös Loránd University in 1985, then he joined the Geophysics Department of the Hungarian Hydrocarbon Research Institute where he dealt with the theoretical modelling of different types of geophysical sondes. Currently he is lecturer in the Institute of Nuclear Technics of the Budapest University of Technology and Economics.



Copyright

Authorization to photocopy items for internal or personal use in research, study or teaching is granted by the Eötvös Loránd Geophysical Institute of Hungary for individuals, instructors, libraries or other non- commercial organizations. We permit abstracting services to use the abstracts of our journal articles without fee in the preparation of their services. Other kinds of copying, such as copying for general distribution, for advertising or promotional purposes, for creating new collective works, or for resale are not permitted. Special requests should be addressed to the Editor. There is no charge for using figures, tables and short quotes from this journal for re-publication in scientific books and journals, but the material must be cited appropriately, indicating its source.

Az Eötvös Loránd Geofizikai Intézet hozzájárul ahhoz, hogy kiadványainak anyagáról belső vagy személyes felhasználásra kutatási vagy oktatási célokra magánszemélyek, oktatók, könyvtárak vagy egyéb, nem kereskedelmi szervezetek másolatokat készítsenek. Engedélyezzük a megjelentetett cikkek összefoglalóinak felhasználását referátumok összeállításában. Egyéb célú másoláshoz, mint például: terjesztés, hirdetési vagy reklám célok, új, összefoglaló jellegű anyagok összeállítása, eladás, nem járulunk hozzá. Az egyedi kéréseket kérjük a szerkesztőnek címezni. Nem számolunk fel díjat a kiadványainkban szereplő ábrák, táblázatok, rövid idézetek más tudományos cikkben vagy könyvben való újrafelhasználásáért, de az idézés pontosságát és a forrás megjelölését megkivánjuk.